Potassium Cation Affinities of Matrix Assisted Laser Desorption Ionization Matrices Determined by Threshold Collision-Induced Dissociation: Application to Benzoic Acid Derivatives

S. D. M. Chinthaka and M. T. Rodgers*

Department of Chemistry, Wayne State University, Detroit, Michigan 48202

Received: October 12, 2006; In Final Form: June 2, 2007

Threshold collision-induced dissociation of K^+(*x*BA) complexes with xenon is studied using guided ion beam mass spectrometry. The *x*BA ligands studied include benzoic acid and all of the mono- and dihydroxy-substituted benzoic acids: 2-, 3-, and 4-hydroxybenzoic acid and 2,3-, 2,4-, 2,5-, 2,6-, 3,4-, and 3,5-dihydroxybenzoic acid. In all cases, the primary product corresponds to endothermic loss of the intact *x*BA ligand. The cross section thresholds are interpreted to yield 0 and 298 K bond dissociation energies (BDEs) for K^+−*x*BA after accounting for the effects of multiple ion-neutral collisions, the kinetic and internal energy distributions of the reactants, and dissociation lifetimes. Density functional theory calculations at the B3LYP/6-31G* level of theory are used to determine the structures of the *x*BA ligands and their complexes with K^+. Theoretical BDEs are determined from single-point energy calculations at the B3LYP/6-311+G-(2d,2p) and MP2(full)/6-311+G(2d,2p) levels using B3LYP/6-31G* optimized geometries. Four favorable binding modes for the K^+(*x*BA) complexes are found. In all complexes to an *x*BA ligand that does not have a 2-hydroxyl substituent, the most favorable binding mode corresponds to a single interaction with the carbonyl oxygen atom. Formation of a 4-membered ring via chelation interactions with both oxygen atoms of the carboxylic acid group is found to be the most favorable binding mode for all of the 2-hydroxy-substituted systems except K^+(2,3-dihydroxybenzoic acid). In these complexes, a hydrogen-bonding interaction between the hydrogen atom of the carboxylic acid moiety and the oxygen atom of the 2-hydroxy substituent provides additional stabilization. Formation of a 5-membered chelation ring via interaction of K^+ with the oxygen atoms of adjacent hydroxyl substituents is also favorable and corresponds to the ground-state geometry for the K^+(23DHBA) complex. Formation of a 6-membered chelation ring via interaction of K^+ with the carbonyl and 2-hydroxyl oxygen atoms is also quite favorable but does not correspond to the ground-state geometry for any of the systems examined here. The experimental BDEs determined here are in very good agreement with the calculated values.

Introduction

Matrix assisted laser desorption ionization (MALDI) has become a versatile ionization technique for mass analyses of fragile nonvolatile macromolecules. The most significant applications of MALDI are for the accurate determination of the molecular weight and primary sequence of proteins, carbohydrates, and nucleic acids; the molecular mass distribution, repeating units, and end group identification of synthetic polymers;[1] and the characterization of large molecules such as dendrimers,[2−4] nanotubes,[5] and fullerenes.[6] Although MALDI is widely used as a soft ionization method in mass spectrometry, the ionization mechanisms are still poorly understood. Several mechanisms have been proposed to explain the ionization processes that occur in MALDI analyses. The most popular mechanisms proposed to date involve excited-state acid−base chemistry, proton transfer following matrix photoionization, hydrogen atom transfer following analyte photoionization, excited-state salt chemistry, protonation of the sodium salt of the analyte, energy pooling, and gas-phase capture of a cation by the analyte.[7,8]

These ion formation mechanisms can be divided into two categories, ion formation in the condensed phase followed by laser ablation and ion formation in the gas phase after laser ablation. Other experiments suggest that some ions may be formed as a natural consequence of the solid-to-gas-phase transition.[8] Ionization mechanisms involving matrix radical cation formation have also been proposed.[9,10] Ion formation in the condensed phase (i.e., within the sample matrix) can be accurately predicted only on the basis of condensed-phase thermodynamics where many intermolecular interactions influence the binding. In contrast, gas-phase ion formation can be predicted from gas-phase thermodynamics, where only individual isolated interactions occur. However, experimental evidence for gas-phase ion formation has been less reported[11−15] compared to that of the condensed phase.

Cationization, protonation, deprotonation, and electron transfer are the major ionization processes that occur in MALDI via the proposed ionization mechanisms.[16−18] Several reports of experimental and theoretical determinations of gas-phase proton affinities, basicities, and ionization energies of benzoic acid derivatives and commonly used MALDI matrices have been published.[19−22] Studies of cationization processes have also appeared in the literature.[23,24] However, these studies are based on qualitative or semiquantitative studies of cationization of MALDI matrices. Only a limited number of quantitative and theoretical studies of cationization of MALDI matrices have been published.[25−29]

* Corresponding author.

10.1021/jp0667238 CCC: $37.00
Published on Web 08/02/2007

Cationization is largely the result of association of the analyte or matrix molecules with alkali metal cations and is one of the major secondary ionization processes that occur in MALDI. Such cationization can lead to both advantages and disadvantages for mass analyses. Alkali metal cations, primarily sodium and potassium cations, arise from impurities present in matrix chemicals and glassware and from the separation procedures that are carried out to purify analytes. Synthetic polymers are often observed as extensively sodiated or potassiated complexes in MALDI mass spectra.[30−35] In polymer analyses, metal salts are generally intentionally added to MALDI samples to enhance signal intensity. The association of Na^+ and K^+ with the matrix and analyte molecules can be suppressed by adding complementary metal cations that bind more strongly, e.g., Li^+, [36] Cu^{2+}, and Ag^+.[16]

The major disadvantage of cationization by alkali metal cations is that it generally leads to more complicated mass spectra. Cationization reduces the intensity of each of the peaks of interest and makes the mass spectra more crowded with less desirable peaks by spreading the concentration of the analyte (or fragments thereof) over several peaks (sodiated, potassiated, and salt clustered). In extreme cases, cationization is even more problematic because of the association of metal cation clusters with the analyte.[37,38] These clusters of peaks are normally observed as closely spaced bunches of peaks. All of these processes lead to complicated mass spectra and prevent rapid identification and interpretation. Several attempts have been made to reduce or suppress cationization. The addition of ammonium salts to the matrix/analyte mixture, followed by post-crystallization washing with citrate and phosphate buffer solution, has been shown to greatly suppress matrix−alkali metal cation cluster formation.[38] The addition of Li^+ or Cu^{2+},[36] the use of sol−gel-assisted laser desorption ionization,[37] and the use of ionic liquids with popular MALDI matrix anions as matrices[39] have also been shown to reduce the complexity of mass spectra due to alkali metal cation association with the matrix or analytes. However, all reported attempts to improve the quality of mass spectra have evolved on the basis of qualitative observations and empirical studies. Very little thermodynamic data that can be used to predict the cationization behavior in MALDI processes has been reported in the literature.[26,29,40−42] The relative alkali metal cation affinities of both matrix and analyte molecules are needed to understand and predict the ionization processes that will occur in MALDI analyses. Accurate thermodynamic data, that is, cation affinities of both matrices and analyte molecules, would allow MALDI analyses to be carried out in a more controllable manner. However, empirical evidence also suggests that, in addition to the alkali metal cation affinities, structural features of the matrices and analyte also affect the ionization mechanisms.[7]

In this study, the potassium cation affinities and stable binding conformations of K^+ to benzoic acid and all of its mono- and dihydroxy-substituted derivatives are determined. This work is a follow-up to an earlier study,[29] where the analogous Na^+ systems were examined. These ligands were chosen because several are widely used as MALDI matrices[43] and they have also been used experimentally and theoretically to probe and attempt to explain the ionization processes that occur in MALDI analyses.[7,17,44] These molecules are also building blocks for other MALDI matrices. Guided ion beam tandem mass spectrometry techniques are used to collisionally excite complexes of K^+ bound to 10 different benzoic acid derivatives: benzoic acid (BA), 2-hydroxybenzoic acid (2HBA), 3-hydroxybenzoic acid (3HBA), 4-hydroxybenzoic acid (4HBA), 2,3-dihydroxybenzoic acid (23DHBA), 2,4-dihydroxybenzoic acid (24DHBA), 2,5-dihydroxybenzoic acid (25DHBA), 2,6-dihydroxybenzoic acid (26DHBA), 3,4-dihydroxybenzoic acid (34DHBA), and 3,5-dihydroxybenzoic acid (35DHBA). The ground-state structures of the *x*BA matrices along with their calculated dipole moments and isotropic molecular polarizabilities (determined here) are shown in Figure 1. The kinetic energy-dependent cross sections for the collision-induced dissociation (CID) processes are analyzed by methods developed previously.[45,46] The kinetic and internal energy distributions of the reactants, multiple ion-neutral collisions, and the kinetics of unimolecular dissociation are explicitly included in the analyses. Bond dissociation energies (BDEs) of 10 K^+(*x*BA) complexes are derived and compared with values obtained from ab initio and density functional theory. Comparison is also made to values previously reported for the K^+(25DHBA) complex[26] and the analogous Na^+(*x*BA) complexes.[29]

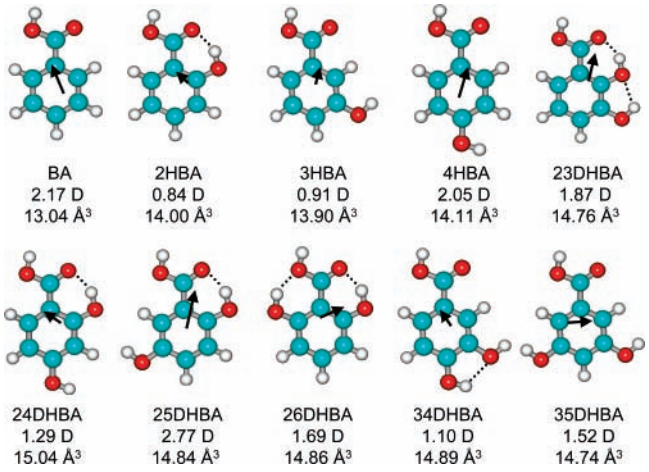

Figure 1. Ground-state geometries of the *x*BA ligands optimized at the B3LYP/6-31G* level of theory. Properly scaled dipole moments (in debyes) are shown as arrows. Calculated isotropic molecular polarizabilities (in cubic angstroms) are also shown. Dipole moments and polarizabilities are taken from theoretical calculations performed here.

Experimental Section

General Procedures. Cross sections for CID of K^+(*x*BA) with Xe, where *x*BA = BA, 2HBA, 3HBA, 4HBA, 23DHBA, 24DHBA, 25DHBA, 26DHBA, 34DHBA, and 35DHBA, were measured as a function of kinetic energy with a guided ion beam tandem mass spectrometer that has been described previously.[47] Potassium cations are generated by glow discharge via Ar^+ sputtering of a tantalum or iron boat containing potassium metal operated at ∼1−2 kV and ∼10−20 mA. The K^+(*x*BA) complexes are formed by condensation of K^+ and the neutral *x*BA ligands in a 1.2 m long flow tube operating at 0.6−0.8 Torr pressure. The *x*BA ligands are introduced by thermal vaporization of solid samples and required heating the neutral *x*BA ligand to between 60 and 170 °C depending upon the extent of substitution and internal hydrogen bonding (i.e., the more highly substituted the *x*BA ligand, the higher the temperature required to vaporize it, and for the xBA ligands having equivalent levels of substitution, those ligands capable of forming internal hydrogen bonds required significantly lower temperatures to vaporize). No evidence that this temperature influenced the internal energy content of the ions emanating from the flow tube source region was observed. The K^+(*x*BA) complexes are collisionally stabilized and thermalized by greater

than 10^5 collisions with the He and Ar bath gases, such that ions emerging from the source region are assumed to have internal energies that are well described by a Maxwell−Boltzmann distribution of rovibrational states at room temperature.

The ions are effusively sampled, focused, accelerated, and focused into a magnetic sector momentum analyzer for reactant ion selection. Mass-selected ions are decelerated to a desired kinetic energy and focused into an octopole ion beam guide. The octopole passes through a static gas cell containing Xe at low pressure (0.05−0.20 mTorr) to ensure that multiple ion-neutral collisions are improbable. The octopole ion guide acts as an efficient radial trap for ions such that scattered reactant and products ions are not lost as they drift toward the end of the octopole.[48−50] The product and unreacted beam ions are focused into a quadrupole mass filter for mass analysis and subsequently detected with a secondary electron scintillation (Daly) detector and standard pulse counting techniques.

Data Handling. The measured product ion intensities are converted to absolute cross sections using a Beers' law analysis as described previously.[46] Absolute uncertainties in the cross section magnitudes are estimated to be ±20% and are largely derived from errors in the pressure measurement and the effective length of the interaction region. Relative uncertainties are ±5%.

Ion kinetic energies in the laboratory frame, E_{lab}, are converted to energy in the center of mass frame, E_{CM}, using the formula $E_{CM} = E_{lab}m/(m + M)$, where M and m are the masses of the ionic and neutral reactants, respectively. All energies reported here are in the center-of-mass frame unless otherwise noted. The absolute zero and distribution of the ion kinetic energies are determined using the octopole ion guide as a retarding potential analyzer as previously described.[46] The distribution of ion kinetic energies is nearly Gaussian with a full width at half-maximum (fwhm) between 0.2 and 0.4 eV (lab) for these experiments. The uncertainty in the absolute energy scale is ±0.05 eV (lab).

Because multiple collisions can influence the shape of CID cross sections and the threshold regions are most sensitive to these effects, each CID cross section was measured twice at three nominal Xe pressures (0.05, 0.10, and 0.20 mTorr). Data free from pressure effects are obtained as previously described.[51,52] Thus, cross sections subjected to thermochemical analysis are the result of single bimolecular encounters.

Theoretical Calculations. To obtain model structures, vibrational frequencies, rotational constants, and energetics for the neutral *x*BA ligands and their complexes to K^+, ab initio and density functional theory calculations were performed using Gaussian 98.[53] Geometry optimizations were performed at the B3LYP/6-31G* level of theory. The optimized structures were used to calculate the vibrational frequencies and rotational constants necessary for modeling of the experimental data. The vibrational frequencies were scaled by a factor of 0.9804 for thermal energy adjustments and modeling of experimental data.[54] The scaled vibrational frequencies are listed in the Supporting Information in Table S1, and the rotational constants are given in Table S2. Single-point energy calculations were performed at the B3LYP/6-311+G(2d,2p) and MP2(full)/6-311+G(2d,-2p) levels of theory with the B3LYP/6-31G* optimized geometries. In previous work, we have found that K^+-ligand BDEs computed at the MP2//MP2 level are typically within 1 kJ/mol of MP2//B3LYP values, and therefore we did not pursue additional geometry optimizations at the MP2(full)/6-31G* level of theory. Zero-point energy (ZPE) and basis-set superposition error (BSSE) corrections were also included.[54] As a result of the multiple orientations possible for the carboxylic acid moiety and the hydroxyl group(s) as well as the multiple favorable K^+ binding sites to these *x*BA ligands, numerous low-energy conformations of these species are possible. Therefore, we carefully consider all possible conformations of the *x*BA ligands and K^+(*x*BA) complexes to determine their relative stabilities and the ground-state conformation of each of these species. In several cases, transition states (TSs) between various conformations of the neutral *x*BA ligands and the K^+(*x*BA) complexes are also calculated to determine the barriers for interconversion to establish whether or not such conformational changes are possible under the experimental conditions employed.

The isotropic molecular polarizabilities of the ground-state conformations of each of the neutral *x*BA ligands were calculated at the PBE0/6-311+G(2d,2p) level of theory using the B3LYP/6-31G* optimized geometries. This level of theory has been shown to provide polarizabilities that are in much better agreement with measured values than the B3LYP/6-311+G-(2d,2p) and MP2(full)/6-311+G(2d,2p) levels of theory employed here for the energetic determinations.[55]

Thermochemical Analysis. The CID cross sections are modeled using an empirical threshold energy law:

$$\sigma(E) = \sigma_0 \sum_i g_i(E + E_i - E_0)^n/E \qquad (1)$$

where σ_0 is an energy-independent scaling factor, E is the relative translational energy of the reactants, E_0 is the threshold for reaction of the ground electronic and rovibrational state, and n is an adjustable parameter that describes the efficiency of kinetic to internal energy transfer.[56] The summation is over the rovibrational states of the reactant ions, i, where E_i is the excitation energy of each rovibrational state and g_i is the relative population of each state ($\Sigma g_i = 1$). The relative reactivity of all rovibrational states, as reflected by σ_0 and n, is assumed to be equivalent.

The Beyer−Swinehart algorithm[57−59] is used to evaluate the density of the rovibrational states and the relative populations, g_i are calculated by a Maxwell−Boltzmann distribution at 298 K, the internal temperature of the reactants. The average internal energy of the ground-state conformation of the neutral *x*BA ligands and K^+(*x*BA) complexes are also included in the Supporting Information, Table 1S. To account for the inaccuracies in the computed frequencies, we have increased and decreased the prescaled frequencies (0.9804) by 10%. The corresponding change in the average vibrational energy is taken to be an estimate of 1 standard deviation of the uncertainty in the vibrational energy (Table 1S).

Statistical theories for unimolecular dissociation (RRKM theory) of the collisionally activated ions are also included in our analyses using a modified form of eq 1 to account for ions that may not have undergone dissociation prior to arriving at the detector ($\sim 10^{-4}$ s) as described in detail elsewhere.[45,60] A loose phase space limit (PSL) TS model located at the centrifugal barrier for the interaction of K^+ with the neutral *x*BA ligand is used as described in detail elseware.[45] The rovibrational frequencies appropriate for the energized molecules and the PSL TSs leading to dissociation are given in the Supporting Information in Tables 1S and 2S.

The model represented by eq 1 is expected to be appropriate for translationally driven reactions[61] and has been found to reproduce CID cross-sections well. The model of eq 1 is convoluted with the kinetic energy distributions of both the reactant K^+(*x*BA) complex and neutral Xe atom, and a nonlinear

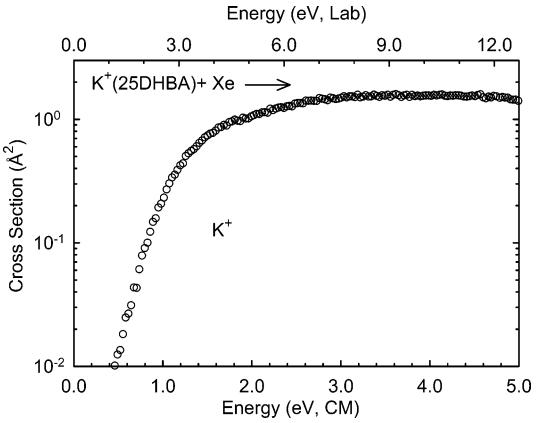

Figure 2. Cross section for collision-induced dissociation of K^+(25DHBA) with Xe as a function of kinetic energy in the center-of-mass frame (lower *x*-axis) and the laboratory frame (upper *x*-axis). Data are shown for a Xe pressure of ~0.2 mTorr.

least-squares analysis of the data is performed to give optimized values for the parameters σ_0, E_0, and n. The error associated with the measurement of E_0 is estimated from the range of threshold values determined for the eight zero-pressure-extrapolated data sets, variations associated with uncertainties in the vibrational frequencies (±10% scaling as discussed above), and the error in the absolute energy scale, 0.05 eV (lab). For analyses that include the RRKM lifetime analysis, the uncertainties in the reported E_0(PSL) values also include the effects of increasing and decreasing the time assumed available for dissociation (10^{-4} s) by a factor of 2.

Equation 1 explicitly includes the internal energy of the reactant ion, E_i. All energy available is treated statistically because the internal energy of the reactants is redistributed throughout the accessible rovibrational energy states of the complex upon collision with Xe. The threshold energies, E_0(PSL), obtained from these analyses are equated to 0 K BDEs because the CID processes examined here are simple noncovalent bond fission reactions that have no barrier in excess of the asymptotic energy.[62,63]

Results

Cross Sections for Collision-Induced Dissociation. Experimental cross sections were obtained for the interaction of Xe with 10 K^+(*x*BA) complexes, where *x*BA = BA, 2HBA, 3HBA, 4HBA, 23DHBA, 24DHBA, 25DHBA, 26DHBA, 34DHBA, and 35DHBA. Figure 2 shows representative data for the K^+(25DHBA) complex. The other K^+(*x*BA) complexes exhibit similar behavior and are included in the Supporting Information as Figure 1S. The most favorable process for all complexes is loss of the intact *x*BA ligand in the CID reactions:

$$K^+(xBA) + Xe \rightarrow K^+ + xBA + Xe \quad (2)$$

Ligand exchange processes to form K^+Xe are also observed as very minor reaction pathways in several of the K^+(*x*BA) systems examined here:

$$K^+(xBA) + Xe \rightarrow K^+Xe + xBA \quad (3)$$

It is likely that this ligand exchange process occurs for all K^+(*x*BA) complexes, but that the signal-to-noise in the other experiments was not sufficient to differentiate the K^+Xe product from background noise. The cross sections for ligand exchange are 2 orders of magnitude smaller than that observed for the corresponding primary CID pathway. At elevated energies, the loss of neutral KOH is observed as a minor dissociation pathway in the CID of the K^+(3HBA) complex. The analogous reaction pathway was not observed for any of the other K^+(*x*BA) complexes.

Threshold Analysis. The model of eq 1 was used to analyze the thresholds for CID reactions (eq 2) in 10 K^+(*x*BA) systems. The results of these analyses are provided in Table 1, and representative results for the K^+(25DHBA) complex are shown in Figure 3. Analyses for the other K^+(*x*BA) complexes are shown in Figure 2S of the Supporting Information. In all cases, the experimental cross sections are accurately reproduced using a loose PSL TS model.[45] Previous work has shown that this model provides the most accurate assessment of the kinetic shifts for CID of electrostatically bound ion−molecule complexes.[45] Good reproduction of the experimental data is obtained over energy ranges exceeding 2.0 eV and cross section magnitudes of at least a factor of 100. Table 1 also includes threshold values, E_0, obtained without inclusion of the RRKM lifetime analysis. The difference between the E_0 and E_0(PSL) threshold values provides a measure of the kinetic shift associated with the finite experimental time window, which should correlate with the density of states at threshold. The kinetic shifts vary between 0.03 and 0.13 eV for these systems. The kinetic shift is the smallest for the K^+(BA) complex, increases for the K^+(HBA) complexes, and increases slightly more for the K^+(DHBA) complexes except K^+(23DHBA) and K^+(26DHBA) complexes, which exhibit somewhat smaller kinetic shifts. This trend is easily understood because the number of vibrational modes available to the complexes increases in that order: 42 for K^+(BA), 45 for the K^+(HBA) complexes, and 48 for the K^+(DHBA) complexes. The smaller kinetic shifts observed for the K^+(23DHBA) and K^+(26DHBA) complexes are likely the result of extensive hydrogen bonding in the complexes and neutrals.

The entropy of activation, $\Delta S^\dagger$, is a measure of the looseness of the TS and also a reflection of the complexity of the system. $\Delta S^\dagger$ is largely determined by molecular parameters used to

TABLE 1: Modeling Parameters of Eq 1 and Entropies of Activation at 1000 K of K^+(*x*BA)[a]

reactant cation	σ_0[b]	n[b]	E_0[c] (eV)	E_0(PSL) (eV)	kinetic shift (eV)	$\Delta S^\dagger$(PSL), J mol^{-1} K^{-1}
K^+(BA)	27.4 (1.7)	1.1 (0.1)	0.98 (0.03)	0.95 (0.03)	0.03	15 (2)
K^+(2HBA)	9.7 (0.5)	1.1 (0.1)	1.12 (0.04)	1.05 (0.03)	0.07	15 (2)
K^+(3HBA)	15.4 (1.0)	1.1 (0.1)	1.09 (0.06)	1.02 (0.04)	0.07	18 (2)
K^+(4HBA)	4.4 (0.1)	1.2 (0.1)	1.16 (0.04)	1.07 (0.03)	0.09	18 (2)
K^+(23DHBA)	5.3 (1.4)	1.0 (0.1)	1.10 (0.06)	1.01 (0.04)	0.09	23 (2)
K^+(24DHBA)	11.2 (1.7)	1.1 (0.1)	1.23 (0.08)	1.12 (0.03)	0.11	15 (2)
K^+(25DHBA)	1.7 (0.1)	1.2 (0.1)	1.17 (0.03)	1.05 (0.02)	0.12	16 (1)
K^+(26DHBA)	29.3 (1.7)	1.1 (0.1)	1.06 (0.04)	1.00 (0.02)	0.06	23 (2)
K^+(34DHBA)	8.8 (0.6)	1.1 (0.1)	1.20 (0.14)	1.08 (0.09)	0.12	19 (2)
K^+(35DHBA)	1.9 (0.1)	1.2 (0.1)	1.15 (0.04)	1.02 (0.03)	0.13	22 (2)

[a] Uncertainties are listed in parentheses. [b] Average values for loose PSL transition state. [c] No RRKM analysis.

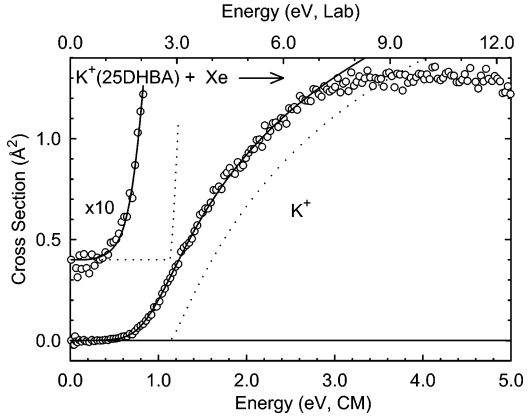

Figure 3. Zero-pressure-extrapolated cross-section for collision-induced dissociation of K^+(25DHBA) with Xe in the threshold region as a function of kinetic energy in the center-of-mass frame (lower *x*-axis) and the laboratory frame (upper *x*-axis). (—) Best fit to the data using the model of eq 1 convoluted over the neutral and ion kinetic and internal energy distributions. (•••) Model cross section in the absence of experimental kinetic energy broadening for reactants with an internal temperature of 0 K.

model the energized molecule and TS for dissociation, but also depends on the threshold energy. The $\Delta S^{\ddagger}$(PSL) values at 1000 K are listed in Table 1 and vary from 15 to 23 J K^{-1} mol^{-1} across these systems. These entropies are indicative of relatively weakly bound complexes that dissociate via loose transition states, as modeled.

Theoretical Results. Theoretical structures and relative stabilities of the various conformers of the neutral *x*BA ligands and K^+(*x*BA) complexes as well as theoretical BDEs for the K^+(*x*BA) complexes were calculated as described in the Theoretical Calculations Section.

Neutral *x*BA Ligands. As mentioned in the Introduction, this work is a follow-up to an earlier study, where we examined the analogous Na^+(*x*BA) systems.[29] As this work involves the same 10 *x*BA ligands, only a brief summary of the theoretical results for these neutral ligands is given here. The ground-state conformations of all 10 *x*BA ligands along with their calculated dipole moments and isotropic molecular polarizabilities are shown in Figure 1. In all cases, the ground-state structures are nearly planar with the carboxylic hydrogen atom oriented away from the phenyl ring. Whenever possible, intramolecular hydrogen bonds form between adjacent substituents and help stabilize the neutral *x*BA ligands. The geometry-optimized structures, calculated dipole moments, and relative stabilities (including ZPE corrections) of all of the stable conformations of the neutral *x*BA ligands are provided in the Supporting Information, Figure 3S. The factors that influence the relative stabilities of the various conformations available to these *x*BA ligands, i.e., intramolecular hydrogen bonding interactions, π resonance stabilization, and steric repulsion between atoms on adjacent substituents, have been discussed in detail previously.[29]

K^+(*x*BA) Complexes. Four distinct very favorable K^+ binding modes of the *x*BA ligands are found and shown schematically for several of the *x*BA ligands in Figure 4. Stable binding geometries in which K^+ binds to a single hydroxyl oxygen atom also exist but are significantly less favorable than the other four binding modes. For example, for the K^+(3HBA) complex, binding of K^+ to the carbonyl oxygen atom of the carboxylic acid moiety (mode A, Figure 4) is 48.9 kJ/mol more favorable at the B3LYP level of theory than binding to the 3-hydroxyl oxygen atom. Similar differences in the stabilities of such binding modes are expected for the other K^+(*x*BA)

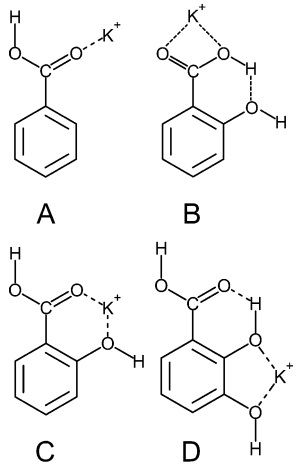

Figure 4. The four energetically favorable stable binding modes of K^+ to the *x*BA ligands. Binding mode A is shown for the K^+(BA) complex but is possible for all 10 *x*BA ligands. Binding modes B and C are shown for the K^+(2HBA) complex but are possible for all 2-hydroxy-substituted *x*BA ligands. Binding mode D is shown for the K^+(23DHBA) complex but is also possible for the 34DHBA ligand.

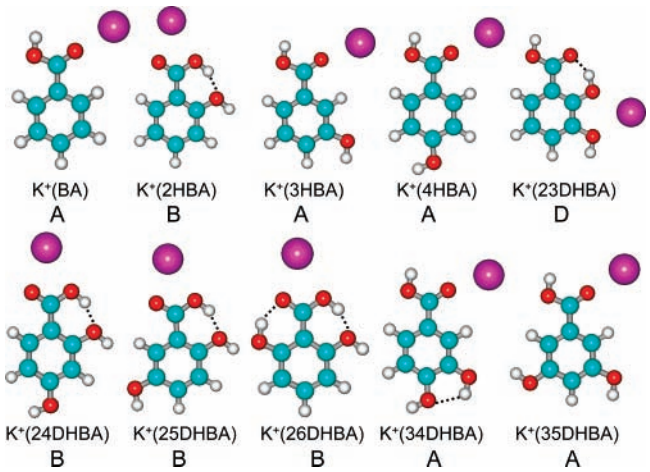

Figure 5. Ground-state geometries of the K^+(*x*BA) complexes optimized at the B3LYP/6-31G* level of theory.

complexes and therefore were not pursued in detail. The ground-state conformations of all 10 K^+(*x*BA) complexes are shown in Figure 5. In all cases except BA, the neutral *x*BA ligand undergoes a change in conformation to achieve optimal binding to K^+ (compare Figures 1 and 5). All low-energy conformations of the K^+(*x*BA) complexes that might be expected to be populated under our experimental conditions, i.e., 298 K internal energy distribution and therefore within 10 kJ/mol of the ground-state structures, and their relative stabilities are also provided in the Supporting Information in Figure 4S.

Theoretical BDEs for the ground-state and low-energy conformations of the K^+(*x*BA) complexes calculated at the B3LYP/6-311+G(2d,2p) and MP2(full)/6-311+G(2d,2p) levels of theory (using geometries optimized at the B3LYP/6-31G* level of theory and assuming that the complexes dissociate to produce the neutral *x*BA ligand in its ground-state conformation) are summarized along with the measured values in Table 2. The calculated energies of these K^+(*x*BA) complexes, the *x*BA ligands, and K^+ are provided in the Supporting Information in Tables 3S and 4S.

Two different favorable binding modes were found for binding of K^+ to BA. In the ground-state conformation, K^+ binds directly to the carbonyl oxygen of carboxylic acid moiety

TABLE 2: Measured and Calculated Enthalpies of Potassium Cation Binding to *x*BA at 0 K[a]

	experiment		theory, MP2[b]			theory, B3LYP[c]		
K^+(*x*BA)	TCID	binding mode	D_e	D_0[d]	$D_{0,BSSE}$[e]	D_e	D_0[d]	$D_{0,BSSE}$[e]
K^+(BA)	92.3 (2.6)	A1	94.6	92.7	88.6	99.3	97.4	96.5
		B1	93.0	92.1	88.0	93.8	92.9	92.1
K^+(2HBA)	101.5 (2.6)	B1	99.0	99.1	94.3	96.8	96.7	96.0
		C1	92.8	91.8	85.8	89.8	88.7	87.5
K^+(3HBA)	99.2 (3.6)	A1	97.7	95.9	91.7	101.4	99.6	98.8
		A2	94.2	92.8	88.6	98.5	97.1	96.2
		A3	93.0	91.4	87.2	97.3	95.7	94.9
		B1	93.4	93.4	90.5	94.8	94.8	94.0
		B2	94.0	93.2	88.9	94.7	93.9	93.1
		B3	91.6	90.8	88.0	92.4	91.7	91.0
		A4	86.8	85.4	81.2	91.6	90.2	89.4
K^+(4HBA)	103.4 (2.8)	A1	99.8	97.7	93.5	106.3	104.2	103.3
		A2	97.4	95.3	91.1	104.2	102.1	101.3
		B1	97.8	96.9	92.6	100.6	99.7	98.9
		B2	96.9	96.0	91.8	99.6	98.7	98.0
K^+(23DHBA)	98.2 (4.1)	D1	107.4	105.7	100.2	102.5	100.8	99.8
		B1	100.2	100.2	95.7	98.5	98.6	97.8
		C1	99.6	98.7	92.7	96.9	95.9	94.7
K^+(24DHBA)	108.3 (3.2)	B1	102.0	102.0	97.3	100.5	100.4	99.6
		B2	97.9	98.1	93.6	96.3	96.5	95.7
		C1	95.9	94.8	89.4	93.8	92.6	91.4
K^+(25DHBA)	101.5 (2.4)	B1	100.8	101.2	96.8	99.0	99.4	98.6
		B2	100.3	100.6	95.9	98.6	98.9	98.1
		C1	95.0	94.0	89.4	92.7	91.7	90.5
		C2	94.5	93.6	88.2	92.1	91.2	90.0
K^+(26DHBA)	96.4 (2.3)	B1	108.4	107.8	103.0	107.0	106.4	105.4
K^+(34DHBA)	104.3 (8.4)	A1	102.2	100.1	95.9	106.8	104.8	103.9
		A2	98.5	96.6	92.4	105.0	103.1	102.2
		A3	93.0	91.2	87.1	101.4	99.8	98.9
		B1	97.0	96.2	92.0	99.9	99.1	98.3
		B2	98.2	97.2	92.8	99.8	98.8	97.9
		B3	97.1	96.3	92.0	98.4	97.7	96.9
		A4	90.4	88.7	84.6	97.7	96.1	95.4
K^+(35DHBA)	99.1 (2.5)	A1	97.8	96.0	91.8	101.3	99.5	99.1
		A2	96.0	94.6	90.4	99.7	98.3	97.5
		B1	94.1	92.9	88.7	95.0	93.8	93.1
		B2	93.5	92.4	88.1	94.6	93.4	92.7
		A3	88.1	86.7	82.5	92.7	91.3	90.4
AEU/MAD[f]	3.4 (1.8)		4.8 (3.6)	5.2 (3.2)	7.5 (3.2)	4.9 (3.6)	4.0 (3.6)	3.9 (3.7)

[a] Values are given in kilojoules per mole. Uncertainties are listed in parentheses. [b] Calculated at the MP2(full)/6-311+G(2d,2p) level of theory using B3LYP/6-31G* optimized geometries and assuming that the complex dissociates to the ground state neutral conformer. [c] Calculated at the B3LYP/6-311+G(2d,2p) level of theory using B3LYP/6-31G* optimized geometries assuming that the complex dissociates to the ground state neutral conformer. [d] Also includes ZPE corrections with frequencies scaled by 0.9804. [e] Also includes BSSE corrections. [f] Average experimental uncertainty (AEU) and mean absolute deviation (MAD) between the measured and calculated values.

(binding mode A, Figure 4). The C═O−K^+ bond angle is nearly linear but shifted slightly away from the hydroxyl group. An alternative binding mode is possible when the hydrogen atom of the carboxylic acid moiety is oriented toward the phenyl ring, thereby allowing K^+ to interact with both oxygen atoms of the carboxylic acid moiety and forming a 4-membered chelation ring (binding mode B, Figure 4). The relative stability of the A and B conformations of K^+(BA) depends upon the level of theory employed. B3LYP calculations favor A over B by 4.5 kJ/mol, while MP2 calculations suggest a smaller difference in stability, with A favored over B by only 0.6 kJ/mol. In the B conformer, steric repulsion between the hydrogen atom of the carboxylic acid moiety and the ortho hydrogen atom of the phenyl ring causes the carboxylic acid moiety to rotate out of the plane by 16.2°. This leads to a reduction in the stability gained via resonance delocalization of the carbonyl π electrons with those of the aromatic ring, and costs ~25.4 kJ/mol as estimated from the relative stabilities of the corresponding conformers of neutral BA (at the B3LYP level of theory). The favoring of binding mode A over B suggests that the enhanced binding associated with the formation of the 4-membered chelation ring (as compared to a single interaction with the carbonyl oxygen atom) provides just slightly less stabilization than the energetic cost associated with the loss of π electron delocalization, or about 20.9 kJ/mol (at the B3LYP level of theory). The interconversion of the A and B conformers of neutral BA is not feasible because the TS for this interconversion lies 45.7 kJ/mol higher in energy than the ground-state conformer (at the B3LYP level of theory), almost 3 times as large as the internal energy of BA at 298 K, the internal temperature of the reactants (Table 1S).[29] However, complexation to K^+ facilitates this geometry change by providing the energy associated with complexation (96.5 kJ/mol at the B3LYP level of theory, Table 2).

The preference for binding mode A over B is found for all the K^+(*x*BA) complexes that do not possess a 2-hydroxyl group, i.e., K^+(BA), K^+(3HBA), K^+(4HBA), K^+(34DHBA), and K^+(35DHBA) complexes for both B3LYP and MP2

TABLE 3: Enthalpies and Free Energies of Potassium Cation Binding to *x*BA at 0 and 298 K[a]

K^+(*x*BA)	ΔH_0	ΔH_0[b]	$\Delta H_{298} - \Delta H_0$[b]	ΔH_{298}	ΔH_{298}[b]	$T\Delta S_{298}$[b]	ΔG_{298}	ΔG_{298}[b]
K^+(BA)	92.3 (2.6)	96.5	0.2 (0.8)	92.5 (2.7)	96.7	25.4 (4.2)	67.1 (5.0)	71.3
K^+(2HBA)	101.5 (2.6)	96.0	0.5 (1.0)	102.0 (2.8)	96.5	25.8 (4.0)	76.2 (4.9)	70.7
K^+(3HBA)	99.2 (3.6)	98.8	0.4 (0.9)	99.6 (3.7)	99.2	25.8 (4.0)	73.8 (5.4)	73.4
K^+(4HBA)	103.4 (2.8)	103.3	0.4 (0.8)	103.8 (2.9)	103.7	25.8 (4.2)	78.0 (5.1)	77.9
K^+(23DHBA)	98.2 (4.1)	99.8	0.6 (1.1)	98.8 (4.2)	100.4	29.2 (4.0)	69.6 (5.8)	71.2
K^+(24DHBA)	108.3 (3.2)	99.6	−0.4 (1.0)	107.9 (3.4)	99.2	26.6 (4.0)	81.3 (5.2)	72.6
K^+(25DHBA)	101.5 (2.4)	98.6	−0.7 (0.9)	100.8 (2.6)	97.9	26.5 (4.2)	74.3 (4.9)	71.4
K^+(26DHBA)	96.4 (2.3)	105.4	−0.1 (0.9)	96.3 (2.5)	105.3	27.8 (4.1)	68.5 (4.8)	77.5
K^+(34DHBA)	104.3 (8.4)	103.9	0.3 (0.9)	104.6 (8.4)	104.2	27.3 (4.2)	77.3 (9.4)	76.9
K^+(35DHBA)	99.1 (2.5)	99.1	0.3 (0.8)	99.4 (2.6)	99.4	27.8 (4.2)	71.6 (4.9)	71.6

[a] Values are given in kilojoules per mole. Uncertainties are listed in parentheses. [b] Density functional theory values from calculations at the B3LYP/6-311+G(2d,2p) level of theory using B3LYP/6-31G* optimized geometries with frequencies scaled by 0.9804.

calculations. For all of the hydroxy- and dihydroxy-substituted systems, several low-energy A and B conformers are found that differ only in the relative orientations of the carboxylic acid moiety and hydroxyl groups (compare Figures 5 and 4S). Although not explicitly calculated, interconversion of the A and B conformers in these latter systems should also be facile because complexation to K^+ provides a similar amount of energy as for the BA system (96.5 to 103.9 kJ/mol at the B3LYP level of theory, Table 2). The energy required for interconversion of the A- and B-type conformers of these systems is expected to be similar to that calculated for K^+(BA) because the hydroxyl groups are distant from the carboxylic acid moiety and therefore should not significantly impact such interconversion. In all cases where binding mode B is favored over A [i.e., K^+(2HBA), K^+(23DHBA), K^+(24DHBA), K^+(25DHBA) and K^+(26DHBA)], this preference arises as a result of hydrogen-bonding interactions between the carboxylic acid moiety (either carbonyl or hydroxyl group) and the 2-hydroxyl substituent.

The calculations find three very favorable binding modes for K^+ to 2HBA: a single binding interaction with the carbonyl oxygen atom (mode A, Figure 4); 4-membered chelation ring formation with both oxygen atoms of the carboxylic acid group (mode B, Figure 4); and 6-membered chelation ring formation between K^+ and the oxygen atoms of carboxylic acid and 2-hydroxyl groups (mode C, Figure 4). For 2HBA, mode B is significantly favored over mode A because, although both binding geometries require that the hydrogen bond between the carbonyl oxygen atom and the 2-hydroxyl hydrogen atom be broken, a new hydrogen bond between the hydrogen atom of the carboxylic acid moiety and the 2-hydroxyl oxygen atom is formed in the B conformer. Mode B is calculated to be 8.0 kJ/mol more favorable than mode C for binding of K^+ to 2HBA (B3LYP calculations). In the ground-state conformation of neutral 2HBA, there is a strong hydrogen bond (23.4 kJ/mol at the B3LYP level of theory) between the carbonyl oxygen and hydroxyl hydrogen atoms. To allow 6-membered ring formation, this hydrogen bond must be broken and the hydroxyl group must rotate 180°. This creates a relatively large activation energy barrier of ~54 kJ/mol as compared to the ground state of neutral 2HBA (at the B3LYP level of theory). The interconversion of the B and C conformers is clearly feasible because the exothermicity of K^+ binding (96.0 kJ/mol at the B3LYP level of theory) easily exceeds the energy barrier. The favoring of binding mode B over C suggests that the enhanced binding associated with the formation of the 6-membered chelation ring (as compared to the 4-membered ring) provides slightly less stabilization than the energetic cost associated with breaking the hydrogen bond between the between the carbonyl oxygen and hydroxyl hydrogen atoms, or about 15.4 kJ/mol (at the B3LYP level of theory). Several other stable but less energetically favorable binding conformations are also possible. However, the relative stabilities of such conformations are such that they are unlikely to be accessed under our experimental conditions and thus will not be discussed further.

The preference for binding mode B over C is found for all of the 2-hydroxy-substituted systems: K^+(2HBA), K^+(23DHBA), K^+(24DHBA), K^+(25DHBA), and K^+(26DHBA) for both B3LYP and MP2 theories. The energy difference between the most favorable B and C conformers is smallest for K^+(23DHBA), 2.7 kJ/mol, and somewhat larger and fairly similar for the K^+(2HBA), K^+(24DHBA), and K^+(25DHBA) complexes, 7.7−8.0 kJ/mol, but is significantly larger for the K^+(26DHBA) complex, 25.3 kJ/mol (at the B3LYP level of theory). A possible reason for the larger difference observed for the K^+(26DHBA) system is that the B conformer is stabilized by two hydrogen bonds rather than a single hydrogen bond (as is the case for the other complexes), which likely leads to greater electron delocalization that must be given up to form the C conformer.

The calculations find another very favorable binding mode for K^+ to 23DHBA, where K^+ binds to the oxygen atoms of the adjacent 2- and 3-hydroxyl substituents and forms a 5-membered chelation ring (binding mode D, Figure 4). This conformer is further stabilized by a hydrogen bond between the carbonyl oxygen and 2-hydroxyl hydrogen atoms. This D conformer is found to be the ground-state geometry for the K^+(23DHBA) complex and is favored over the most stable B and C conformers by 2.2 and 4.9 kJ/mol (B3LYP) and 5.5 and 7.0 kJ/mol (MP2), respectively. Binding mode D is also possible for 34DHBA. However, without the enhanced stability gained by hydrogen bond formation that occurs for K^+(23DHBA), conformer D is less favorable than the various A and B conformers. B3LYP calculations find that conformer D of K^+(34DHBA) lies 22.5 kJ/mol above the ground-state A conformer, whereas MP2 calculations suggest that it is somewhat more stable and lies 11.2 kJ/mol above the ground-state structure.

Conversion from 0 to 298 K. To allow comparison to literature values and commonly used experimental conditions, we convert the measured and B3LYP calculated BDEs determined here at 0 K into 298 K bond enthalpies and free energies. The enthalpy and entropy conversions are calculated using standard formulas and the vibrational and rotational constants determined for the B3LYP/6-31G* optimized geometries given in Tables 1S and 2S. Table 3 provides the 0 and 298 K enthalpy, free energy, and enthalpic and entropic corrections for all the systems based upon the ground-state conformations of both the K^+(*x*BA) complex and *x*BA ligand. The theoretical values listed in Table 3 correspond to those determined at the B3LYP level of theory, as this provides better agreement with the measured values than the MP2 results, and is therefore deemed more reliable; see below. Uncertainties in the enthalpic and entropic

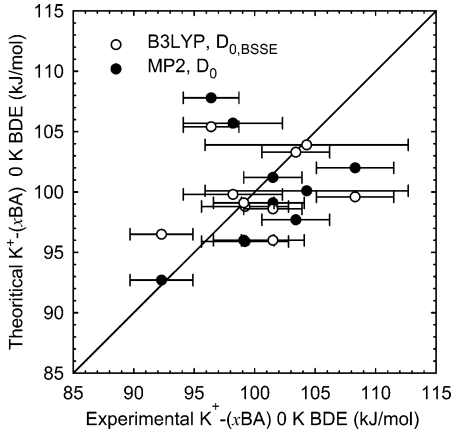

Figure 6. Theoretical versus TCID experimental K^+-xBA BDEs (in kilojoules per mole). All values are at 0 K and are taken from Table 2; the B3LYP values (○) include BSSE corrections, while the MP2 values (●) do not. The diagonal line indicates the values for which calculated and measured BDEs are equal.

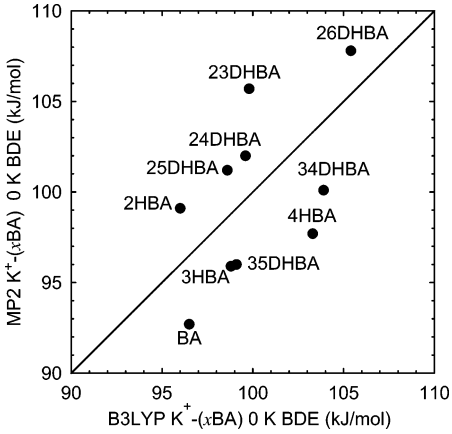

Figure 7. Comparison of the MP2 and B3LYP calculated BDEs of K^+(*x*BA) complexes (in kilojoules per mole). All values are at 0 K and are taken from Table 2; the B3LYP values include BSSE corrections, while the MP2 values do not. The diagonal line indicates the values for which the MP2 and B3LYP BDEs are equal.

corrections are determined by 10% variation in all molecular constants and additionally by 50% variation in the metal−ligand frequencies. Such scaling provides a reasonable estimate of the computational errors in these modes, while the latter is the dominant source of the uncertainties listed here. Thermal corrections were also computed for all of the low-lying excited conformations of the K^+(*x*BA). The order of relative stability among the various low-energy conformations for all of the K^+(*x*BA) complexes at 298 K is unchanged from that at 0 K.

Discussion

Comparison of Theoretical and Experimental Results. The BDEs of the 10 K^+(*x*BA) complexes measured here at 0 K are summarized in Table 2. Also listed in Table 2 are the corresponding theoretical BDEs for all low-energy conformers calculated at the B3LYP/6-311+G(2d,2p) and MP2(full)/311+G(2d,2p) levels of theory. The agreement between the theoretical (B3LYP and MP2 theories) and measured BDEs is illustrated in Figure 6. As can be seen in Figure 6, the agreement between the measured and at least one of the theoretical BDEs is very good for most complexes, but both theories lie outside of the experimental uncertainly for the K^+(24DHBA) and K^+(26DHBA) systems. The mean absolute deviation (MAD) between the experimental BDEs and those for the ground-state conformations calculated at the B3LYP level of theory for all 10 K^+(*x*BA) complexes is 3.9 ± 3.7 kJ/mol, slightly higher than the average experimental uncertainty (AEU) of 3.4 ± 1.8 kJ/mol in these measurements. MP2 theory does not perform quite as well and provides BDEs that are generally lower that the experimental values. The MAD between MP2 theory and experiment is 7.5 ± 3.2 kJ/mol, and decreases to 5.2 ± 3.2 kJ/mol when BSSE corrections are not included. It has previously been suggested that BSSE corrections overestimate the effect associated with the differing sizes of the basis sets used to calculate the complexes verses dissociation products and can lead to binding energies that are too low, particularly for MP2 theory.[64] In our previous study of the corresponding Na^+(*x*BA) complexes, similar behavior was also observed but was even more pronounced because BSSE corrections generally scale with the binding energy. It is interesting to note that, in most cases, B3LYP theory does a better job describing the bonding in these K^+(*x*BA) complexes than MP2. However, in several cases, MP2 outperforms B3LYP theory. Thus, the B3LYP and MP2 (no BSSE corrections) calculated BDEs are compared in Figure 7. As can be seen in the figure, the MP2 BDEs of systems having a 2-hydroxy substituent are greater than those found with B3LYP theory. In contrast, the opposite trend is found for systems without a 2-hydroxy substituent, where the B3LYP BDEs exceed those computed with MP2 theory. This behavior suggests that while both levels of theory do a reasonable job of describing the binding in these systems, neither produces the systematic trends in binding expected among these systems.

Nature of the K^+-xBA Interaction. As discussed above, the dominant dissociation pathway observed in the interaction of the K^+(*x*BA) complexes with Xe is simple CID to produce K^+ and the neutral *x*BA ligand. In addition, theoretical calculations suggest that the binding primarily arises from interactions of K^+ with the lone pair(s) of electrons on the oxygen atom(s) of the carboxylic acid moiety and/or the hydroxyl substituents. Therefore, the binding in these complexes is largely electrostatic, arising from ion−dipole and ion-induced dipole interactions. The effects of the hydroxyl substituents upon the binding may be examined by comparing the *x*HBA and *x*DHBA ligands to BA. The addition of hydroxyl groups increases the polarizability of the ligands. The polarizability of the ground-state conformation of neutral BA is calculated to be 13.04 Å^3; it increases to between 13.90 and 14.11 Å^3 for the *x*HBA ligands and increases further to between 14.74 and 15.04 Å^3 for the *x*DHBA ligands. As can be seen in Figure 1, the polarizability varies only slightly with the position(s) or orientations of the hydroxyl substituents. Therefore, the ion-induced dipole attractions should roughly correlate with the extent of hydroxylation. This trend was clearly seen in our previous study of the interactions of Na^+ with these same ligands.[29] However, this trend is not quite as evident for the K^+(*x*BA) systems. Because K^+ is larger than Na^+, the M^+-O bonds are longer in the K^+(*x*BA) complexes than in the analogous Na^+(*x*BA) complexes. The primary effect of the longer M^+-O bonds is weaker binding. The effect on the binding produced by the small enhancement of the ion-induced dipole interaction upon hydroxylation of BA or HBA appears to be of a similar size or even smaller than the experimental error in these measurements. Ion−dipole interactions should also be important in determining the binding in these complexes. The ion−dipole attractions should correlate with the dipole moments of these ligands. However, the dipole moments of these ligands are very sensitive to conformation. In many cases, very similar theoretical BDEs are calculated for different conformations and binding geometries. Thus, both the magnitude of the

dipole moment and its projection along the binding direction must be considered. The dipole moment of the neutral *x*BA ligand appropriate for binding mode A is generally relatively low. However, a single linear interaction of K^+ with the carboxylic acid oxygen atom provides maximum overlap and thus a strong interaction is achieved. When K^+ binds to the *x*BA ligands via binding mode B, the dipole moment of the neutral ligand is much larger and the chelation interactions lead to stronger binding, thereby favoring mode B over A. However, steric repulsion between the ortho hydrogen atom and the carboxylic hydrogen atom (ligands without a 2-hydroxyl group) makes these conformations (mode B) less stable than mode A. Indeed, this behavior is found for the complexes of BA, 3HBA, 4HBA, 34DHBA, and 35DHBA. In the 2-hydroxy-substituted ligands, mode B is likely favored over mode A because, although both binding geometries require that the hydrogen bond between the carbonyl oxygen atom and the 2-hydroxyl hydrogen atom be broken, a new hydrogen bond between the hydrogen atom of the carboxylic acid moiety and the 2-hydroxyl oxygen atom is formed in the B conformers. The preference of mode B over C for the 2-hydroxy-substituted *x*BA ligands suggests that formation of the 4-membered chelation ring coupled with retention of a hydrogen-bonding interaction provides more stability than 6-membered chelation ring formation.

Comparison to Literature Values. The present experimental results are also compared to those of Zenobi and co-workers,[26] who measured the gas-phase potassium basicities (GK^+B) of four commonly used MALDI matrices, including 25DHBA, using equilibrium and reaction kinetic methods in a Fourier transform ion cyclotron resonance (FT-ICR) mass spectrometer. They measured a GK^+B for 25DHBA of 99 ± 2 kJ/mol, while their theoretical calculations at the B3LYP/6-31+G* level of theory provide a GK^+B of 69.4 kJ/mol. To compare these results with those obtained in this study, GK^+Bs must be converted to 0 K potassium ion affinities, GK^+A (i.e., $\Delta G_{298} \rightarrow \Delta H_0$). Using the thermal corrections determined here, their measured value corresponds to a GK^+A or BDE for the K^+(25DHBA) complex of 126 ± 4 kJ/mol, while the calculated value is 96.4 kJ/mol. The BDE of the K^+(25DHBA) complex measured here is 101.5 ± 2.4 kJ/mol, almost 25 kJ/mol lower the value determined by Zenobi and co-workers. Similarly, the values calculated here at the B3LYP/6-311+G(2d,2p)//B3LYP/6-31G* and MP2(full)/6-311+G(2d,2p)//B3LYP/6-31G* levels of theory are 99.4 and 100.6 kJ/mol, respectively, when BSSE corrections are not included, in excellent agreement with the value measured here. Moreover, our theoretical and experimental values are in good agreement with the theoretical value determined by Zenobi and co-workers (96.4 kJ/mol). Therefore, the level of theory employed cannot explain the discrepancy in the measured values.

Zenobi and co-workers tried to explain the discrepancy between their theoretical and experimental values by assuming that during the cation transfer reaction, the conformation of 25DHBA does not change; i.e., that K^+(25DHBA) dissociates to an excited-state asymptote such that the measured value corresponds to a diabatic BDE. Our calculations indicate that this conformation of 25DHBA lies 38.4 kJ/mol higher in energy than the ground-state conformation (Supporting Information, Figure 3S). Thus our calculations suggest a diabatic BDE for K^+(25DHBA) of 136.5 kJ/mol at the B3LYP level of theory. This value is in excellent agreement with the theoretical value for diabatic dissociation reported by Zenobi and co-workers, 138.5 kJ/mol. However, the calculated diabatic BDEs are still 10−12 kJ/mol higher than the experimental value measured by Zenobi and co-workers, 126 ± 4 kJ/mol. Thus, the appropriate interpretation of their measured value is still uncertain.

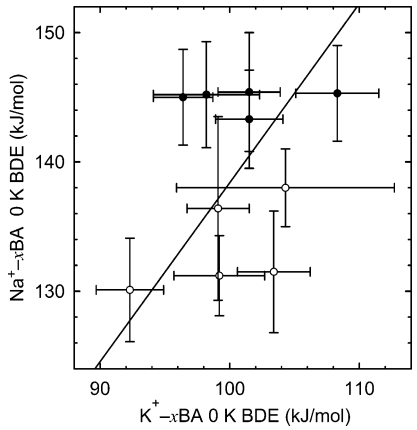

Figure 8. Comparison of measured BDEs of K^+(*x*BA) and Na^+(*x*BA) complexes (in kilojoules per mole). The K^+−*x*BA BDEs are taken from Table 2, while the Na^+−*x*BA values are taken from our previous study.[29] A linear regression fit to all of the data is shown and provides a slope of 1.375. (●) 2-Hydroxy-substituted *x*BA ligands; (○) *x*BA ligands with a 2-hydroxyl group.

The assumption that 25DHBA retains the same geometry it possesses in the K^+(25DHBA) complex after dissociation may be reasonable for the study performed by Zenobi and co-workers because the measured values are determined via cation transfer reaction kinetics and equilibrium methods. In these methods, the reference base must be chosen such that the difference in GK^+B is small enough to rapidly achieve equilibrium and provide measurable populations of both the K^+(25DHBA) and $K^+(B_{ref})$ complexes. This requirement generally means that the GK^+B values must be within about 10 kJ/mol. Therefore, sufficient energy to overcome the barrier to conformational changes may not be available and true equilibrium cannot be achieved. In contrast, threshold CID (TCID) measurements performed here lead to the ground-state neutral conformation of 25DHBA because the barrier to the conformational change is much smaller than the enthalpy of dissociation. Therefore, the present study directly measures the adiabatic BDE. The adiabatic 0 K BDEs for these K^+(*x*BA) complexes are given in Table 2, while adiabatic 298 K BDEs and GK^+B values are reported in Table 3.

Comparison to Na^+ Affinities. In previous work, we determined the Na^+ affinities of all 10 of the *x*BA ligands examined here.[29] Those results are compared to the present results in Figure 8. A linear regression analysis of these data provides a slope of 1.375, indicating that Na^+ binds 37.5% more strongly than K^+ to these *x*BA ligands. The primary reason for the enhanced binding is that Na^+ is smaller than K^+. The nonlinear distance dependencies of the electrostatic interactions that control the binding in these complexes fall off rapidly, as R^{-2} for an ion-aligned dipole and R^{-4} for ion-induced dipole interactions, resulting in weaker binding interactions in the complexes to the larger alkali metal cation, K^+. The larger size of K^+ not only leads to weaker binding but also alters the preferred binding geometries in the complexes to the *x*BA ligands that have a 2-hydroxy substituent. Na^+ forms a very stable 6-membered chelation ring with the 2-hydroxy-substituted ligands. In contrast, K^+ is considerably larger and binds less strongly. As a result, the K^+(*x*BA) complexes involving ligands with a 2-hydroxy substituent achieve greater stability by preserving the hydrogen-bonding interaction and forming a 4-membered chelation ring with the oxygen atoms of the

carboxylic acid moiety. As can be seen in Figure 8, the Na^+ and K^+ affinities of these *x*BA ligands are not highly correlated. In general, the BDEs increase with increasing hydroxylation, but the minor variations in the BDEs with structure differ for the Na^+ and K^+ complexes. The 2-hydroxy-substituted systems show greater relative variation in their BDEs to K^+ than to Na^+ (Figure 8, ●), whereas those systems without a 2-hydroxy substituent exhibit more systematic behavior. Thus, a likely reason for the less than optimal correlation is that the mode of binding for half of these systems differs from the Na^+(*x*BA) to the corresponding K^+ (*x*BA) complex.

Implications for MALDI Analyses. As discussed in the Introduction, the relative alkali metal cation affinities of both matrix and analyte molecules are needed to understand and predict the ionization processes that will occur in MALDI analyses. In turn, the availability of such thermochemical data will help facilitate rational optimization of MALDI analyses. The thermodynamic data reported here and in our previous study of the Na^+ affinities of these *x*BA ligands begin to provide the information needed for the optimization of MALDI analyses. The high temperatures and pressures that occur within the MALDI plume provide sufficient internal energy to the vaporized matrix molecules to overcome barriers to conformational relaxation. Therefore, the adiabatic values measured here are likely to be more relevant to actual MALDI conditions than the apparent diabatic values reported by Zenobi and co-workers and thus provide thermochemical data needed to understand and optimize MALDI cationization processes. However, the sodium and potassium cation affinities of the analytes of interest are also necessary and are the subject of additional studies being pursued in our laboratory.

In addition to the relative cation binding affinities of the matrix and analyte molecules, structural features of the matrix must also be considered to achieve control over the ionization processes in MALDI analyses.[7] Thus the structural information derived from the theoretical calculations performed here is also useful for understanding and optimizing MALDI analyses. As described by Zenobi and Knochenmuss,[17] compounds that exhibit an excited-state proton-transfer mechanism (ESPT) must possess a hydroxyl group ortho to a carbonyl moiety [i.e., $-C(O)CH_3$, $-C(O)OH$, or $-C(O)NH_2$] that forms a hydrogen bond with the carbonyl oxygen atom. Upon photon absorption, the hydroxyl proton is transferred to the carbonyl oxygen, increasing the acidity of the hydrogen atom and thereby facilitating proton transfer. Among the *x*BA ligands examined here, half possess a 2-hydroxyl group (i.e., 2HBA, 23DHBA, 24DHBA, 25DHBA, and 26DHBA). We previously found that Na^+ prefers to bind to these 2-hydroxy-substituted benzoic acids via binding mode B (a 6-membered chelation ring between the carbonyl and the 2-hydroxyl oxygen atoms). To accommodate the sodium cation, the hydroxyl hydrogen atom rotates away from the carbonyl oxygen atom, thereby breaking the hydrogen bond. This structural change blocks the ESPT mechanism and prevents proton transfer between the hydroxyl and carbonyl groups. Karbach and Knochenmuss[65] have shown that 25DHBA is not always ESPT-active; the presence of Na^+ diminishes the ESPT activity. When K^+ is complexed to 25DHBA, it retains the hydrogen-bonding interaction and binds to the ligand via formation of a 4-membered chelation ring to the oxygen atoms of the carboxylic acid moiety. While such binding would still likely diminish proton transfer between the 2-hydroxyl group and the carboxylic acid moiety, it should not completely shut it down. Therefore, the presence of K^+ may reduce the efficiency of proton transfer between the matrix and analyte molecules but should not eliminate this ionization pathway for 25DHBA or structurally related matrices. In contrast, the presence of Na^+ will likely eliminate proton-transfer ionization of the analyte by such matrices.

On the basis of the structural and energetic factors that influence cationization in MALDI analyses, it will be preferable to choose a matrix that binds cations more strongly than the analyte and for which cation binding does not shut down proton-transfer mechanisms to minimize cationization/maximize protonation of the analyte. In contrast, it will be preferable to choose a matrix with a lower cation affinity than the analyte and potentially one that interferes with proton-transfer ionization to maximize cationization of the analyte. Because Na^+ binds more strongly than K^+ and shuts down the ESPT transfer pathway in the 2-hydroxy-substituted benzoic acid ligands, it can be more effectively employed with these matrices to favor cationization of the analyte, particularly for analyte molecules having sodium cation affinities that exceed that of the matrix used.

Conclusions

The kinetic energy dependence of the CID of K^+(*x*BA), where *x*BA includes benzoic acid and all mono- and dihydroxy-substituted benzoic acids, with Xe are examined in guided ion beam tandem mass spectrometer. The dominant dissociation process in all cases is loss of the intact *x*BA ligand. Thresholds for these processes are determined after consideration of the effects of reactant kinetic and internal energy distributions, multiple collisions with Xe, and lifetime effects. To obtain molecular constants needed for modeling experimental data and to facilitate appropriate interpretation of experimental results, ab initio calculations at the B3LYP/6-311+G(2d,2p)//B3LYP/6-31G* and MP2(full)/6-311+G(2d,2p)//B3LYP/6-31G* levels of theory are performed. Very good agreement between experimentally determined K^+ affinities and B3LYP values is found in most cases. The agreement between MP2 theory and experiment is not quite as good but is still quite reasonable when BSSE corrections are not included. Various binding modes and the relative dipole moments of the various conformations available to these *x*BA ligands are major factors that govern the strength of binding to K^+. Theoretical calculations suggest that there are four very favorable K^+ binding modes to these *x*BA ligands. However, only two binding modes are represented in the ground state geometries of 9 of the 10 K^+(*x*BA) complexes. Binding mode A, a single direct interaction with the lone pair of electrons on the carbonyl oxygen, is favored for the complexes with BA, 3HBA, 4HBA, 34DHBA, and 35DHBA, while binding mode B, formation of a 4-membered chelation ring with both oxygen atoms of the carboxylic acid group, is favored for the complexes with 2HBA, 24DHBA, 25DHBA, and 26DHBA. The stability of these K^+(*x*BA) complexes is enhanced by additional intramolecular hydrogen bonds whenever possible, and in particular, leads to the preference for mode B over A and C for the 2-hydroxy-substituted *x*BA ligands. The absolute BDEs measured here for the K^+(*x*BA) complexes provide reliable anchors for the potassium cation affinity scale. These thermochemical data, combined with structural information obtained from theoretical calculations, provide insight into means by which the ionization processes that occur in MALDI can be effectively controlled.

Acknowledgment. This work was supported by the National Science Foundation, Grant CHE-0518262.

Supporting Information Available: Tables of vibrational frequencies, average vibrational energies at 298 K, rotational constants of K^+(*x*BA) and *x*BA in their ground-state conformations, and MP2(full)/6-311+G(2d,2p) and B3LYP/6-311+G(2d,2p) energies of all low-energy conformers of K^+(*x*BA) and ground-state conformers of *x*BA; and figures showing cross sections for CID of K^+(*x*BA) with Xe, as well as empirical fits to the primary products channels, optimized geometries, dipole moments, and relative energies of all stable conformations of the neutral *x*BA ligands, and all low-energy conformers of the K^+(*x*BA) complexes (PDF). This material is available free of charge via the Internet at http://pubs.acs.org.

References and Notes

(1) Mowat, I. A.; Donavan, R. J.; Maier, R. J. *Rapid Commun. Mass Spectrom.* **1997**, *11*, 89.

(2) Blais, J. C.; Turrin, C. O.; Caminade, A. M.; Majoral, J. P. *Anal. Chem.* **2000**, *72*, 5097.

(3) Chessa, G.; Scrivanti, A.; Seraglia, R.; Traldi, P. *Rapid Commun. Mass Spectrom.* **1998**, *12*, 1533.

(4) Paupaiboon, U.; Taylor, R. T. *Rapid Commun. Mass Spectrom.* **1999**, *13*, 508.

(5) Xu, S.; Li, Y.; Zou, H.; Jieshan, Q.; Gou, Z.; Gou, B. *Anal. Chem.* **2003**, *75*, 6191.

(6) Fati, D.; Leeman, V.; Vasil'ev, V. Y.; Drewello, T.; Leyh, B.; Hungerbühler, H. *J. Am. Soc. Mass Spectrom.* **2002**, *13*, 1448.

(7) Liao, P.-C.; Allison, J. *J. Mass Spectrom.* **1995**, *30*, 408.

(8) Karbach, V.; Knochenmus, R.; Zenobi, R. *J. Am. Soc. Mass Spectrom.* **1998**, *9*, 1226.

(9) Kinsel, G. M.; Schaffter, L. M. P.; Kinsel, G. R.; Russell, D. H. *J. Am. Chem. Soc.* **1997**, *119*, 2534.

(10) Ehring, H.; Karas, M.; Hillenkamp, F. *Org. Mass Spectrom.* **1992**, *27*, 472.

(11) Rashidezadeh, H.; Guo, B. *J. Am. Soc. Mass Spectrom.* **1998**, *9*, 724.

(12) Lehmann, E.; Knochenmus, R.; Zenobi, R. *Rapid Commun. Mass Spectrom.* **1997**, *11*, 1483.

(13) Lienes, C, F.; O'Malley, R. M. *Rapid Commun. Mass Spectrom.* **1992**, *6*, 564.

(14) Dean, P. A.; O'Malley, R. M. *Rapid Commun. Mass Spectrom.* **1993**, *7*, 53.

(15) Thomson, B.; Suddaby, K.; Rubin, A.; Lajole, G. *Eur. Polym. J.* **1996**, *32*, 239.

(16) Scrivens, J. H.; Jackson, A. T.; Yates, H. T.; Green, M. R.; Critchley, G.; Brown, J.; Bateman, R. H.; Bowers, M. T.; Gidden, J. *Int. J. Mass Spectrom. Ion Process.* **1997**, *165/166*, 363.

(17) Zenobi, R.; Knochenmuss, R. *Mass Spectrom. Rev.* **1998**, *17*, 337.

(18) Knochenmuss, R.; Stortelder, A.; Breuker, K.; Zenobi, R. *J. Mass Spectrom.* **2000**, *35*, 1237.

(19) Burton, R. D.; Watson, C. H.; Eyler, J. R.; Lang, G. L.; Powell, D. H.; Avery, M. Y. *Rapid Commun. Mass Spectrom.* **1997**, *11*, 443.

(20) Steenvoorden, R. J. J. M.; Bruker, K.; Zenobi, R. *Eur. Mass Spectrom.* **1997**, *3*, 339.

(21) Breuker, K.; Knochenmuss. R.; Zenobi, R. *Int. J. Mass Spectrom.* **1999**, *184*, 25.

(22) Yassin, F. H.; Marynick, D. S. *Mol. Phys.* **2005**, *103*, 183.

(23) Wong, C. K. L.; Chan, T.-W. D. *Rapid Commun. Mass Spectrom.* **1997**, *11*, 517.

(24) Fujii, T. *Mass Spectrom. Rev.* **2000**, *19*, 111.

(25) Zhang, J.; Knochenmuss, R.; Stevenson, E.; Zenobi, R. *Int. J. Mass Spectrom.* **2002**, *213*, 237.

(26) Zhang, J.; Dyachokva, E.; Ha, T. K.; Knochenmuss, R.; Zenobi, R. *J. Phys. Chem. A* **2003**, *107*, 6891.

(27) Zhang, J.; Ha, T.-K.; Knochenmuss, R.; Zenobi. R. *J. Phys. Chem. A* **2002**, *106*, 6610.

(28) Ohanessian, G. *Int. J. Mass Spectrom.* **2002**, *219*, 577.

(29) Chinthaka, S. D. M.; Chu, Y.; Rannulu, N. S.; Rodgers, M. T. *J. Phys. Chem. A* **2006**, *110*, 1426.

(30) Rashidzadeh, H.; Wang, Y.; Guo, B. *Rapid Commun. Mass Spectrom.* **2000**, *14*, 439.

(31) Hoberg, A. M.; Haddleton, D. M.; Derrick, P. J. *Eur. Mass. Spectrom.* **1997**, *3*, 471.

(32) Knochenmuss, R.; Lehmann, E.; Zenobi, R. *Eur. Mass Spectrom.* **1998**, *4*, 421.

(33) Rashidezadeh, H.; Guo, B. *J. Am. Soc. Mass Spectrom.* **1998**, *9*, 724.

(34) Rashidezadeh, H.; Hung, K.; Guo, B. *Eur. Mass Spectrom.* **1998**, *4*, 429.

(35) Nielen, M. W. F. *Mass Spectrom. Rev.* **1999**, *18*, 309.

(36) North, S.; Okafo, G.; Birrell, H.; Haskins, N.; Camilleri, P. *Rapid Commun. Mass Spectrom.* **1997**, *11*, 1635.

(37) Chen, W. Y.; Chen, Y. C. *Anal. Chem.* **2003**, *75*, 4223.

(38) Smirnov, I. P.; Zhu, H.; Taylor, T.; Haung, Y.; Ross, P.; Papayanopoulos, I. A.; Martin, S. A.; Pappin, D. J. *Anal. Chem.* **2004**, *76*, 2958.

(39) Mank, M.; Stahl, B.; Boehm, G. *Anal. Chem.* **2004**, *76*, 2938.

(40) Zhang, J.; Ha, T. K.; Knochenmuss, R.; Zenobi, R. *J. Phys. Chem. A* **2002**, *106*, 6610.

(41) Ehlers, A. W.; de Koster, C. G.; Meier, R. J.; Lammertsma, K. *J. Phys. Chem. A* **2001**, *105*, 8691.

(42) Zenobi, R.; Knochenmuss, R. *Mass Spectrom. Rev.* **1998**, *17*, 337.

(43) Krause, J.; Stoeckli, M.; Schlunegger, U. P. *Rapid Commun. Mass Spectrom.* **1996**, *10*, 1927.

(44) Chiarelli, M. P.; Sharkey, A. G., Jr.; Hercules, M. D. *Anal. Chem.* **1993**, *65*, 307.

(45) Rodgers, M. T.; Ervin, K. M.; Armentrout, P. B. *J. Chem. Phys.* **1997**, *106*, 4499.

(46) Ervin, K. M.; Armentrout, P. B. *J. Chem. Phys.* **1985**, *83*, 166.

(47) Rodgers, M. T. *J. Phys. Chem. A* **2001**, *105*, 2374.

(48) Teloy, E.; Gerlich, D. *Chem. Phys.* **1974**, *4*, 417.

(49) Gerlich, D. Diplomarbeit, University of Freiburg, Federal Republic of Germany, 1971.

(50) Gerlich, D. In *State-Selected and State-to-State Ion−Molecule Reaction Dynamics, Part I, Experiment*; Ng, C.-Y., Baer, M., Eds.; Advances in Chemical Physics Series, Vol. 82; Wiley: New York, 1992; p 1.

(51) Dalleska, N. F.; Honma, K.; Sunderlin, L. S.; Armentrout, P. B. *J. Am. Chem. Soc.* **1994**, *116*, 3519.

(52) Schultz, R. H.; Armentrout, P. B. *J. Chem. Phys.* **1992**, *96*, 1046.

(53) Frisch, M. J.; Trucks, G. W.; Schlegel, H. B.; Scuseria, G. E.; Robb, M. A.; Cheeseman, J. R.; Zakrzewski, V. G.; Montgomery, J. A., Jr.; Stratmann, R. E.; Burant, J. C.; Dapprich, S.; Millam, J. M.; Daniels, A. D.; Kudin, K. N.; Strain, M. C.; Farkas, O.; Tomasi, J.; Barone, V.; Cossi, M.; Cammi, R.; Mennucci, B.; Pomelli, C.; Adamo, C.; Clifford, S.; Ochterski, J.; Petersson, G. A.; Ayala, P. Y.; Cui, Q.; Morokuma, K.; Salvador, P.; Dannenberg, J. J.; Malick, D. K.; Rabuck, A. D.; Raghavachari, K.; Foresman, J. B.; Cioslowski, J.; Ortiz, J. V.; Baboul, A. G.; Stefanov, B. B.; Liu, G.; Liashenko, A.; Piskorz, P.; Komaromi, I.; Gomperts, R.; Martin, R. L.; Fox, D. J.; Keith, T.; Al-Laham, M. A.; Peng, C. Y.; Nanayakkara, A.; Challacombe, M.; Gill, P. M. W.; Johnson, B.; Chen, W.; Wong, M. W.; Andres, J. L.; Gonzalez, C.; Head-Gordon, M.; Replogle, E. S.; Pople, J. A. *Gaussian 98*, Revision A.11; Gaussian Inc.: Pittsburgh, PA, 2001.

(54) Foresman, J. B.; Frisch, Æ. *Exploring Chemistry with Electronic Structure Methods*, 2nd ed.; Gaussian: Pittsburgh, PA, 1996.

(55) Smith, S. M.; Markevitch, A. N.; Romanor, D. A.; Li, X.; Levis, R. J.; Schlegel, H. B. *J. Phys. Chem. A* **2000**, *108*, 11063.

(56) Muntean, F.; Armentrout, P. B. *J. Chem. Phys.* **2001**, *115*, 1213.

(57) Beyer, T. S.; Swinehart, D. F. *Comm. Assoc. Comput. Machines*. **1973**, *16*, 379.

(58) Stein, S. E.; Rabinovitch, B. S. *J. Chem. Phys.* **1973**, *58*. 2438.

(59) Stein, S. E.; Rabinovitch, B. S. *Chem. Phys. Lett.* **1977**, *49*, 183.

(60) Khan, F. A.; Clemmer, D. E.; Schultz, R. H.; Armentrout, P. B. *J. Phys. Chem.* **1993**, *97*, 7978.

(61) Chesnavich, W. J.; Bowers, M. T. *J. Phys. Chem.* **1979**, *83*, 900.

(62) Armentrout, P. B.; Simons, J. *J. Am. Chem. Soc.* **1992**, *114*, 8627.

(63) See, for example, Figure 1 in Dalleska, N. F.; Honma, K.; Armentrout, P. B. *J. Am. Chem. Soc.* **1993**, *115*, 12125.

(64) Feller, D. *Chem. Phys. Lett.* **2000**, *322*, 543.

(65) Karbach, V.; Knochenmuss, R. *Rapid Commun. Mass Spectrom.* **1998**, *12*, 968.